FURTHER RESULTS OF SOFT-INPLANE TILTROTOR AEROMECHANICS INVESTIGATION USING TWO MULTIBODY ANALYSES

Pierangelo Masarati[†‡], Giuseppe Quaranta[‡], David J. Piatak[§], Jeffrey D. Singleton[¶], Jinwei Shen[‖]

[‡]Politecnico di Milano, Milano, Italy
[§]NASA LaRC, Hampton, VA
[¶]Army Research Labs, Hampton, VA
[‖]National Institute of Aerospace, Hampton, VA

Abstract

This investigation focuses on the development of multibody analytical models to predict the dynamic response, aeroelastic stability, and blade loading of a soft-inplane tiltrotor wind-tunnel model. Comprehensive rotorcraft-based multibody analyses enable modeling of the rotor system to a high level of detail such that complex mechanics and nonlinear effects associated with control system geometry and joint deadband may be considered. The influence of these and other nonlinear effects on the aeromechanical behavior of the tiltrotor model are examined. A parametric study of the design parameters which may have influence on the aeromechanics of the soft-inplane rotor system are also included in this investigation.

Approach

The objective of this investigation is to develop and refine multibody analytical models to predict the dynamic response, aeroelastic stability, and blade loading of a soft-inplane tiltrotor wind-tunnel model. Comprehensive rotorcraft-based multibody analyses enable modeling of the rotor system to a high level of detail such that complex mechanics and nonlinear effects associated with control system geometry and joint deadband may be considered. The influence of these and other nonlinear effects on the aeromechanical behavior of the tiltrotor model will be examined. A study of the design parameters which have influence on the aeromechanics of the soft-inplane rotor system has been addressed in a previous work, and its prosecution is part of this investigation. This work also focuses on forward-flight configuration analysis, investigating stability results obtained from past experimental campaigns. This research is being performed as a cooperative agreement between the U.S. Army, NASA Langley Research Center, and the University Politecnico di Milano.

A new four-bladed semi-articulated soft-inplane (SASIP) rotor system, designed as a candidate for future heavy-lift rotorcraft, was tested at model scale on the Wing and Rotor Aeroelastic Testing System (WRATS), a 1:5-scale aeroelastic wind-tunnel model based on the V-22. Previous investigations involved a three-blade soft-inplane hub and mainly addressed the stability properties of this configuration [1, 2]. Soft-inplane design implies reduced hub loads and should allow significant weight reduction in large scale tiltrotor aircraft. However, there is significant potential for reduced whirl-flutter stability margins in comparison to the currently exploited stiff-inplane configurations, so extensive aeromechanical investigation is required to determine the feasibility and the requirements of soft-inplane design.

The experimental part of this investigation included a hover test with the model in helicopter mode subject to ground resonance conditions, and a forward flight test with the model in airplane mode subject to whirl-flutter conditions. A three-bladed stiff-inplane gimballed rotor system, used in several previous experiments, was examined under the same conditions as the four-bladed soft-inplane hub to provide a baseline for comparison.

Detailed analytical models of the SASIP tiltrotor have been developed using two multibody rotor codes, one known as MBDyn [Ref. 3] and one known as DYMORE [Ref. 4]. The two codes have similar capabilities, but it is desirable to compare their results (with models created by two different researchers at two different institutions) as a test of robustness for the multibody approach. The multibody analyses include dynamic models for parts of the rotor system which are often not considered in classical rotor analyses, such as the hydraulic actuator control system, the swashplate mechanics (rotating and non-rotating components), pitch links, pitch horns, the

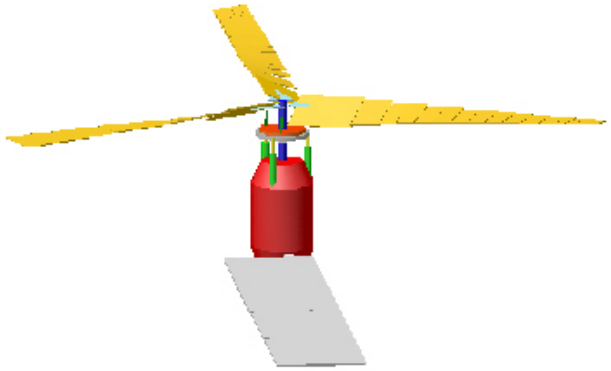

Figure 1: MBDyn multibody model of the three-bladed stiff-inplane tiltrotor system.

rotor shaft and the hub (Fig. 1). The rotor blades are modeled as elastic beams undergoing coupled flap, lag and torsion deformation similar to the finite element methods used in classical rotorcraft analyses.

A third analytical model of the SASIP tiltrotor has been developed using a classical rotorcraft analysis known as UMARC/G, and is based on the UMARC [Ref. 5] comprehensive rotor code. This analysis does not have the capability to model complex joints and extreme nonlinear behavior as do the multibody codes, but is useful to serve as an analytical standard for some portions of the current study.

In Ref. 6 the multibody models were correlated with experimental data from the SASIP model in hover, mainly concerning structural dynamics. The analysis focused on the investigation of the nonlinear behavior of the soft-inplane lead-lag hinge, on the interaction of the rotor motion with the control system, and on ground resonance stability issues. This paper extends that original work to the analysis of forward flight configurations, addressing whirl flutter and load prediction issues.

The paper approaches the problem by directly comparing the results of the two multibody analysis codes, mainly focusing on those that are also available from the experimental campaign described in Ref. 7 and on a selection of test cases that help speeding up model correlation, e.g. modal analysis of the rotor *in vacuo*.

Key Results

Several experiments have been conducted using the SASIP rotor system and its subcomponents [Ref. 7]. The following list presents an overview of tests that are included in the analytical comparisons presented in this paper:

1. Single blade cantilevered outside lag hinge: elastic mode comparison.
2. Single blade mounted on hub in pendulum configuration, flap and lag hinge with lag spring and lag damper included: elastic mode comparison.
3. Control system stiffness calibration: control stiffness and deadband comparison.
4. Pitch-flap coupling and pitch-lag coupling calibration: control system response comparison and analytical models.
5. Hover run-up: fan plot comparisons.
6. Hover performances: thrust, torque and blade angles as functions of collective at prescribed RPM; RPM sweep at prescribed collective setting.
7. Wing structural analysis and hover stability subject to ground resonance conditions: comparison of wing and rotor mode damping and frequencies.
8. Airplane mode stability tests subject to whirl-flutter conditions: comparison of wing and rotor mode damping and frequencies
9. Airplane mode stability issues

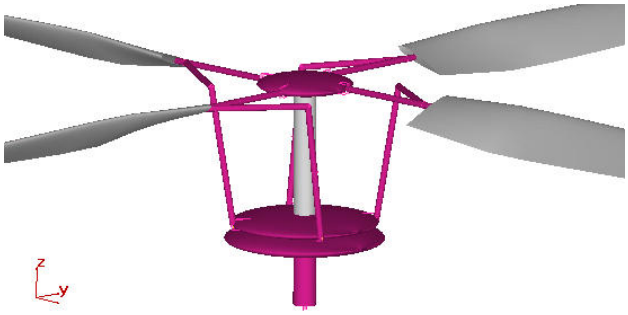

Figure 2: DYMORE model of the SASIP hub setup.

The experimental results for all nine of the listed comparisons have been obtained during several recent test campaigns; many of the data plots required for these comparisons were presented in Ref. 7. The analysis models have been refined through comparison with the experimental data in sequence with the above list.

Some of the key results of this investigation obtained to date are discussed in the following paragraphs. The multibody model developed for the three-bladed stiff-inplane wind-tunnel model is illustrated in Fig. 1. The figure shows the rotor blades, pitch link, swashplate, and hydraulic control actuators which are attached to the pylon, and an elastic wing that is modeled using finite elements. For the SASIP four-bladed rotor system the rotor blades, hub joints, and most of the control system have been developed. Figure 2 shows the DYMORE model of the SASIP setup.

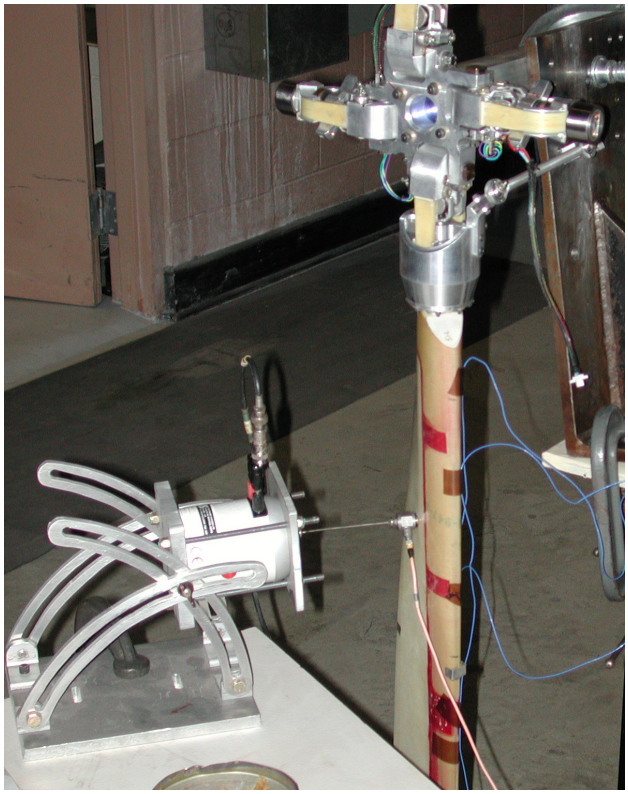

Figure 3: Ground vibration test of an isolated blade.

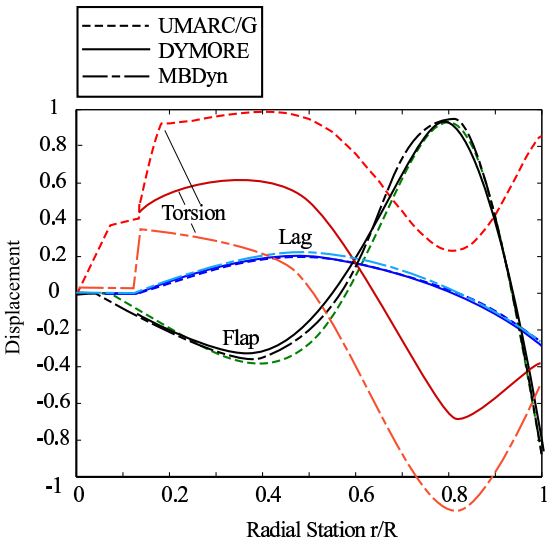

Figure 4: Mode shape comparisons for a non-rotating coupled flap-lag-torsion mode at approximately 64 Hz.

Cantilevered Blade Modal Analysis

A complete review of the blade structural properties has been conducted, to develop a reliable finite element model for subsequent analyses and accurate load recovery. Since both the multibody software codes allow for direct finite element modeling of rotor blades, this analysis permitted the determination of a reasonable trade-off between model accuracy and computational cost, leading to a reduced order model with respect to those used for detailed modal analysis in NASTRAN and UMARC/G.

Table I reports the frequencies of a single blade, cantilevered right outside the lead-lag hinge. MBDyn results refer to a blade model made of 5 parabolic 3 node C^0 beam elements [Ref. 8], with 11 structural nodes. DYMORE results refer to a 4 cubic beam FEM model, while in NASTRAN and UMARC/G 25 beam elements were used.

Hub-Mounted Blade Modal Analysis

A comparison of elastic blade frequencies, for the condition of an isolated blade mounted to the hub (experimental setup shown in Fig. 3), is listed in Table II; the blade pitch is rigidly constrained. This analysis fully exploits the capabilities of multibody software in dealing with the exact kinematics of the articulated blade attachment and of the control system. Different configurations in terms of collective setting, imposed flap or lag angles, lead-lag hinge and pitch link stiffness have been addressed within a single model. The results indicate consistent capabilities of modeling the elastic blade and hinge dynamics among the analyses and generally good agreement with the experimental results. Mode shape comparisons of the three analyses for the fourth mode are shown as an example because this mode has significant participation from flap, lag, and torsion. As shown, the agreement in the flap and lag deflections is excellent, but there is a prediction discrepancy in the torsion participation. This difference in torsion dynamics is currently under investigation.

Control System Calibration

Direct measurements showed that the control system may be regarded as rigid up to the rotating swashplate. Measurable compliance has been detected only between the blade pitch and the swashplate; moreover, an appreciable deadband (± 0.4 deg) results, possibly related to bearing and pitch link ball joints wear. From the multibody analysis standpoint, this has been modeled by concentrating the compliance and the deadband into the rod that represents the pitch link. The resulting analytical equivalent control system stiffness (blade root torsional moment per unit blade pitch) is strongly dependent on the collective setting. Moreover, the experimental data apparently show that there is a strong dependency on the direction the control system is loaded;

Table I: Frequencies of the elastic modes for a single cantilevered blade.

Mode		Frequency, Hz				
No.	**Type**	**Experiment**	**NASTRAN**	**UMARC/G**	**MBDyn**	**DYMORE**
1	F1	10.71	10.61	10.61	10.61	10.45
2	L1	29.20	29.11	29.46	29.03	29.28
3	F2	47.76	51.16	48.99	50.45	50.55
4	T1/F3	107.29	107.23	107.08	107.43	107.28
5	F3/T1	119.07	121.49	119.86	116.78	116.27
6	T2	141.83	177.19	140.19	162.69	166.67

Table II: Frequencies of the elastic modes for a single blade on a fixed hub.

Mode		Frequency, Hz				
No.	**Type**	**Experiment**	**NASTRAN**	**UMARC/G**	**MBDyn**	**DYMORE**
1	F1	0.00	0.00	0.08	0.67	0.11
2	L1	6.46	6.54	6.43	6.32	6.51
3	F2	21.70	19.48	20.06	19.37	19.44
4	F3/L2	61.15	63.12	64.20	62.43	64.30
5	T1	107.94	107.44	103.50	106.58	107.07
6	F4	119.25	91.25	96.21	88.11	92.30

this can be partly related to a significant presence of deadband.

Control System Couplings

The nonlinear modeling capability of the multibody codes is highlighted in Fig. 5, which compares the experimental and predicted pitch-flap coupling response of the rotor system as a function of collective, at zero flap and lag angles. The comparison shows good trends, but a slight difference in magnitude. The control system model is currently being refined to produce a better comparison with the experimental data. It is worth noting that the kinematic couplings also depend on the reference configuration about which they are computed; the only alternative to multibody exact kinematics, with less than ideal accuracy, is represented by pitch, flap and lag tabulation, and 3 parameter table lookup.

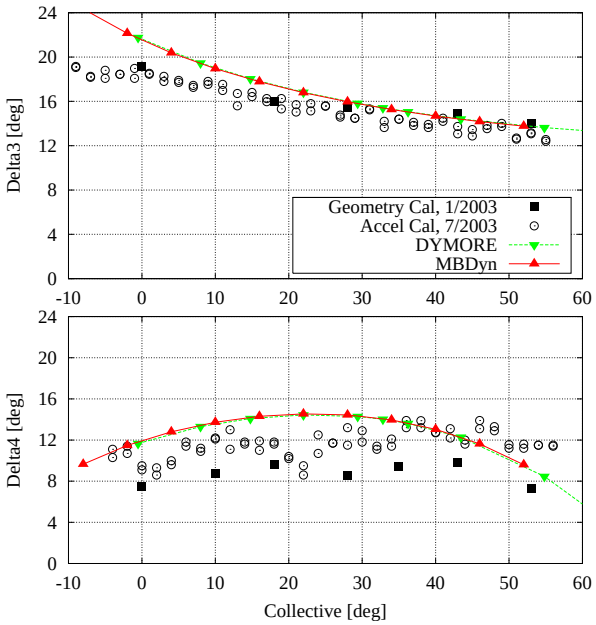

Figure 5: Pitch-flap (δ_3) and pitch-lag (δ_4) coupling comparison between experiment and analysis.

Hover Run-Up

A plot of the regressive rotor lag mode frequencies as function of rotor speed is shown in Fig. 6. The plot shows a difference between the predicted and experimental results, although agreement for the non-rotating condition is good. The lag hinge of the experimental system is a complicated mechanism, and the results obtained thus far represent a simple, constant stiffness equivalent spring hinge joint model. According to simple rigid blade theory, the regressive and the progressive lead-lag frequencies based on root stiffness and rotation

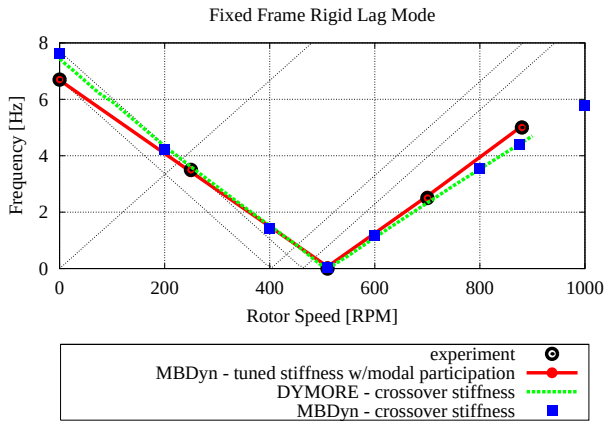

Figure 6: Regressive lead-lag mode frequency variation with rotor speed.

speed is

$$\omega_\xi = \sqrt{\frac{K_\xi}{J_\xi} + \frac{f_\xi S_\xi}{J_\xi}\Omega^2} \pm \Omega$$

No unique lead-lag root stiffness could be found that matches the experimental results over the entire range of rotor RPM; Figure 6 shows the experimental results compared to the best fit obtained by calibrating the lead-lag root spring at the cross-over frequency, compared to those obtainable by calibrating the spring at each RPM. A detailed modal analysis showed a slight participation of blade chordwise bending in the mostly rigid lead-lag mode, resulting in a frequency reduction at 0 RPM of about 3.75%; this required an increase in the spring stiffness by about 7.5%. It is not yet clear what mechanism, if any, relates the lead-lag spring to the rotation speed.

A complete fan plot of the rotor at 10° collective is presented in Fig. 7; some sensitivity of the rotating modes of the rotor to the collective appears at the low angles that are typical of hover; a detailed rotating modal analysis at the higher collective settings of forward flight in a range of angular velocities will be the object of future analysis. The fundamental torsional mode is strongly dependent on the stiffness of the control system; the nominal frequency of about 106 Hz with rigid control system shown in Table II drops to less than 100 Hz when the pitch link is modeled as a deformable rod, according to the calibration described earlier.

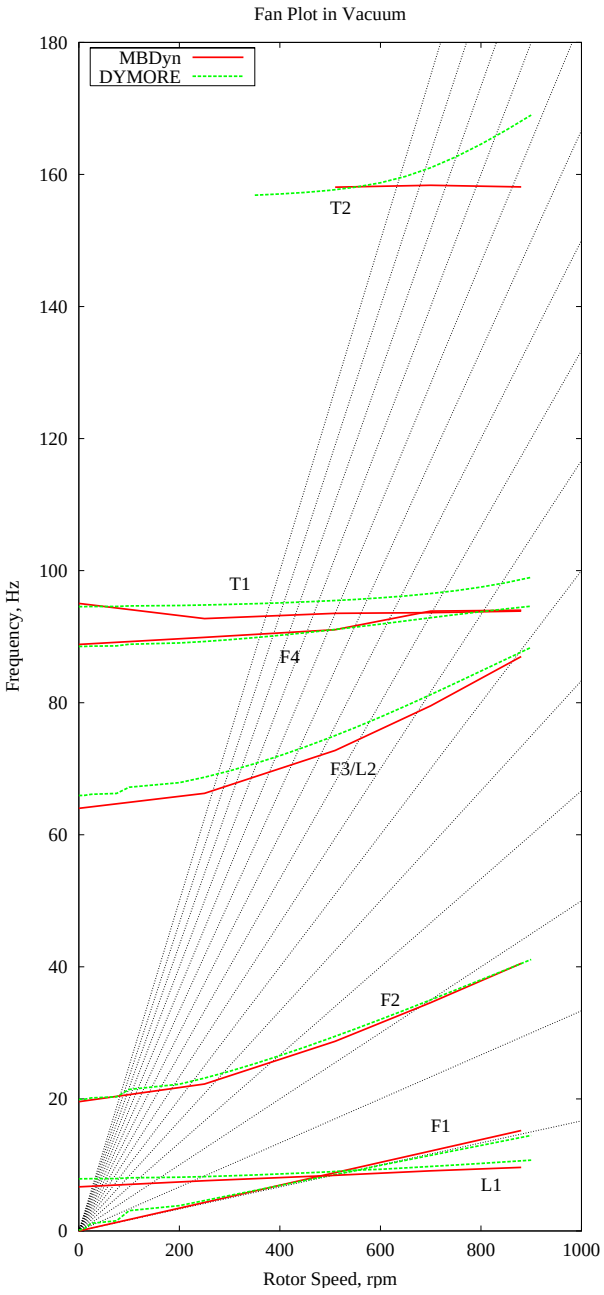

Figure 7: Fan plot of the isolated rotor *in vacuo* at 10° collective; lines: DYMORE, symbols: MBDyn.

Hover Performances

The hover performances of the SASIP rotor are detailed in Figs. 8–17. Experimental results are also shown, whenever available. The figures clearly show how the blade deformability highly affects the rotor per-

formances. This is mostly related to blade torsion as a consequence of the offsets of the normal stress center, of the center of gravity and of the shear center of the blade sections. In fact, it has been verified that by artificially increasing the stiffness of the blade model, the curves shift toward those labeled as "rigid blade". In the multibody analysis, simple uniform inflow was used without any empirical correction, and a standard 2% total tip loss was considered. The thrust was not directly measured, since the WRATS rotor does not have an internal balance; the values in the figures refer to measures of the wing root beam bending moment by means of strain gages, empirically corrected to account for wing download. It is estimated that wing download amounts to 10% of the nominal thrust.

Fig. 13 presents the actual blade pitch angle compared to the input collective. The differences between input and output angles mainly result from the contributions of the flap and lag angles through the control system couplings. While for low input collective the flap and the lag effects are comparable in magnitude but opposed in sign, and thus nearly cancel, for high input collective they add, resulting in an appreciable reduction in actual blade pitch.

Figures 14 and 16 have been corrected by arbitrarily shifting the cone angle, since there were uncertainties on the reference value; Figures 15 and 17 have been corrected as well by arbitrarily shifting the lead-lag angle, since the angle at rest was used as reference, but there is no guarantee that it corresponds to the nominal blade rest azimuthal orientation. It is reasonable to assume that the rest position should be as close as possible to the more critical operating condition from a structural design standpoint, since the main reason for developing soft-inplane tiltrotors is to reduce the hub loads that are typical of stiff-inplane tiltrotors. This can be achieved by carefully tuning the lead-lag hinge chordwise position and the lead-lag spring orientation.

Figs. 16 and 17, reported as a cross-check, show the expected rectilinear behavior that is typical of articulated rotors.

Wing Structural Model and Hover Stability

The wing model, in the case of hover and ground resonance analysis, in absence of significant sources of nonlinear behavior, does not present any peculiar difficulties, as soon as the interaction of the rotor wake with the wing is not a concern. It is essential that the wing behavior, in terms of frequency and modal shapes at the interface with the rotor, is accurately modeled. The multibody formalism allows two different approaches to this problem: (a) the direct finite element modeling of the wing structure, and (b) a modal synthesis of the

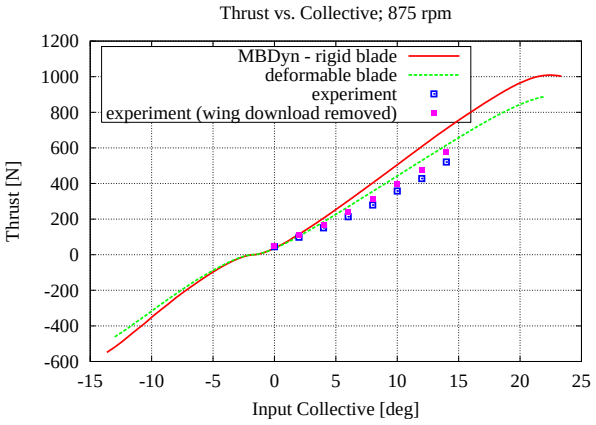

Figure 8: Thrust vs. input collective.

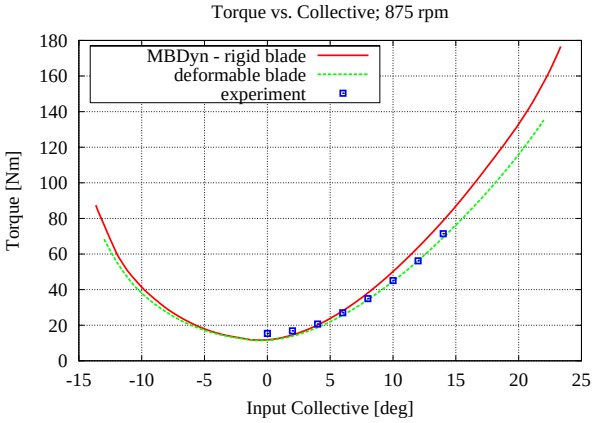

Figure 9: Torque vs. input collective.

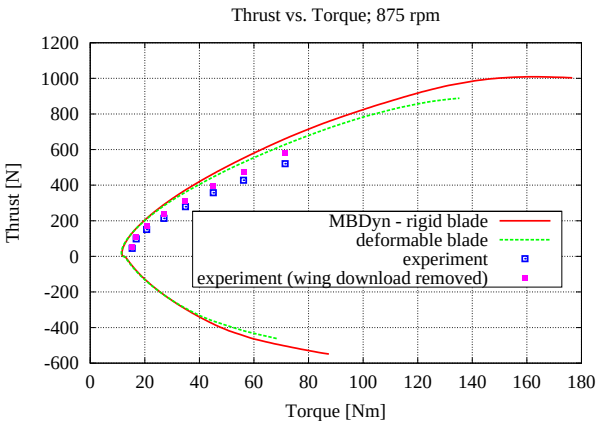

Figure 10: Thrust vs. torque.

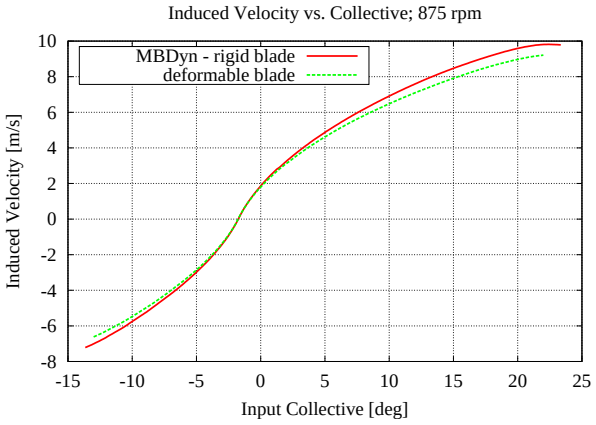

Figure 11: Induced velocity vs. input collective.

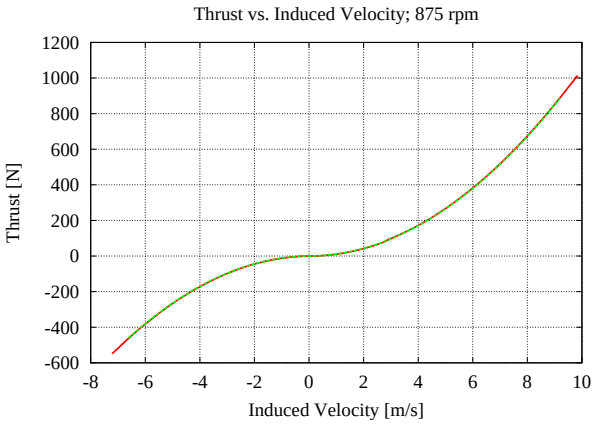

Figure 12: Thrust vs. induced velocity.

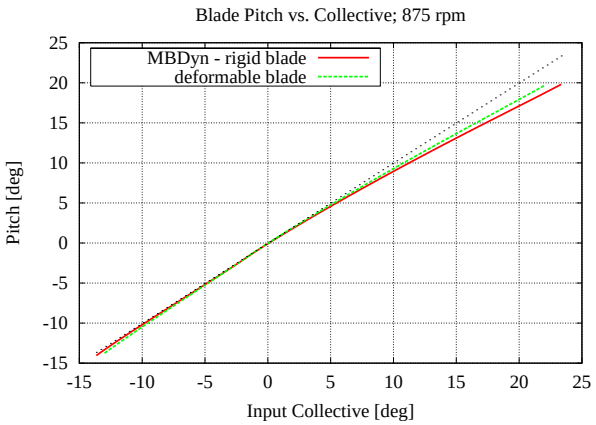

Figure 13: Blade pitch vs. input collective.

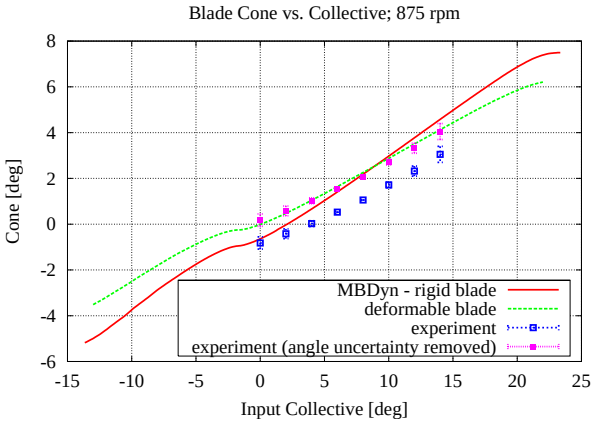

Figure 14: Blade cone vs. input collective.

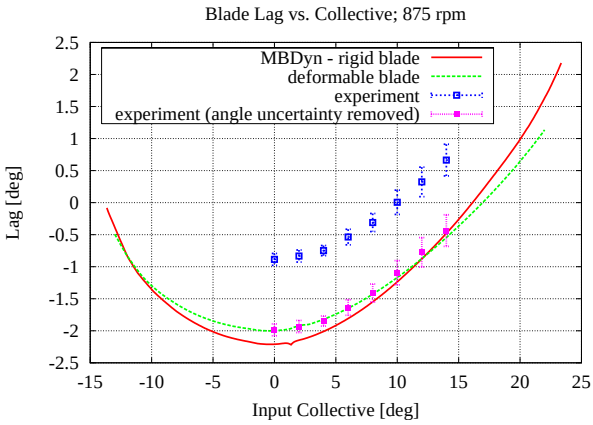

Figure 15: Blade lead-lag vs. input collective.

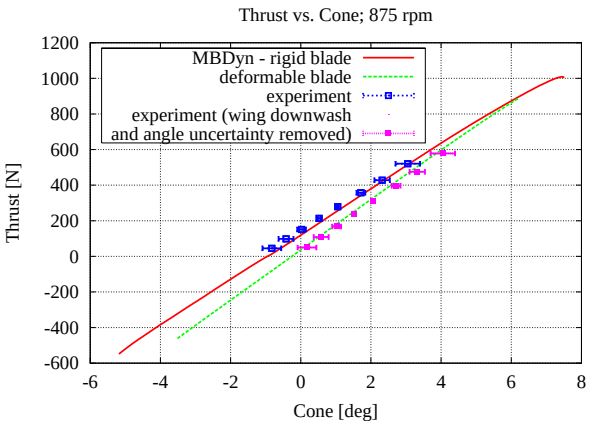

Figure 16: Thrust vs. cone.

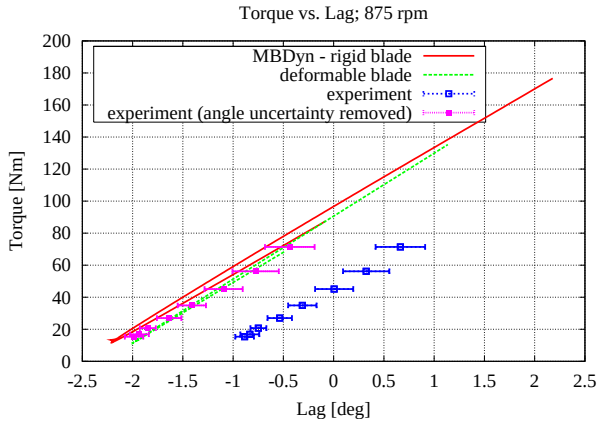

Figure 17: Torque vs. lead-lag angle (positive when lagging).

wing behavior. Within MBDyn both approaches have been considered, while with DYMORE the attention has been focused on the direct FEM modeling.

The hover stability of the SASIP model is a significant issue. In fact, the SASIP experimental system, by design, is prone to ground resonance, because the soft-inplane rotor is mounted on a deformable wing whose fundamental frequencies are right below the non-rotating regressive lead-lag frequency, and the damping of the support, significantly in hover, is inherently delegated to the structure. At the same time, the lead-lag motion of the blades is damped at a nominal damping ration of 10–12%.

Figure 18 shows the lead-lag angle rate that results from a transient analysis of the entire model, with and without aerodynamics, during a linear RPM sweep at a 100 RPM/s rate. It is compared to the plot of some significant system frequencies in the fixed frame. The time and the RPM abscissæ of the two subplots are proportional; this highlights interesting behavior patterns. At about $100 - -200$ RPM there seems to be some interaction between the regressive lead-lag, the progressive flap and the wing beam/chord frequencies. At 510 RPM the rotor speed crosses the lead-lag frequency, resulting in significant resonant response when the aerodynamics are considered. Finally, above 800 RPM the regressive lead-lag frequency crosses again the wing beam/chord mode; this results in ground resonance when aerodynamics are neglected, because no wing structural damping was considered. The aerodynamics seem to provide enough damping to the system to prevent dynamic instabilities.

Airplane Mode Stability

The new four-bladed, soft-inplane rotor system, oriented in airplane mode for high-speed wind-tunnel testing, is shown in Fig. 19 mounted on the WRATS model in the NASA Langley Transonic Dynamics Tunnel (TDT). The basic dynamics of the wing/pylon/rotor system shifts substantially with conversion to airplane mode, as the mass offset of the pylon/rotor moves from above to forward of the elastic axis, and thus creates a significant coupling between the wing beam and torsion modes and the rotor lag mode. The wing chord mode becomes predominantly isolated from these modes in the airplane configuration.

For airplane-mode aeroelastic stability testing, the rotor system is normally operated windmilling (unpowered and disconnected from the drive system), with the collective blade pitch used to adjust the rotor speed, and there is near-zero torque at the rotor shaft. This represents the most conservative manner to test the stability of the system (no damping from the drive system). Under windmilling operation, damping of the key mode associated with system stability (the wing beam mode) was determined to be significantly less for the new four-bladed soft-inplane hub than for the three-bladed stiff-inplane (baseline) system, as shown in Figure 21 (from Ref. 7). Damping of the wing beam mode was generally less than 1.0% in windmilling flight for all the soft-inplane configurations considered (on-downstop (D/S), off-D/S; 0.57/rev dampers, 0.63/rev dampers; 550, 742, and 888 RPM rotor speeds). In powered-mode (200 in-lb torque maintained, ∼22.6 Nm) the system damping and the stability boundary are known to increase significantly, as reported in Ref. 7.

Figure 23 shows the frequency and the damping of the wing beam mode at 748 rpm in off- and on-D/S configuration. The numerical values and trends are compared to the results from the wind tunnel campaign described in Ref. 7.

The DYMORE model has been calibrated based on Ground Vibration Tests (GVT) and wind-tunnel model setup concerning mode frequencies and damping. A structural damping, resulting in 0.65% damping of the wing beam bending mode, was used to match non-rotating GVT tests. This, in conjunction with the damping from the wing aerodynamics, leads to the fairly good agreement with wind-tunnel measurements presented in Figure 23.

The MBDyn model, instead, uses a modal superelement to describe the wing and pylon deformability, based on a previously validated NASTRAN modal analysis in GVT configuration. The boundary mass method has been used to produce accurate modes and modal masses and stiffnesses, because the simplicity of the

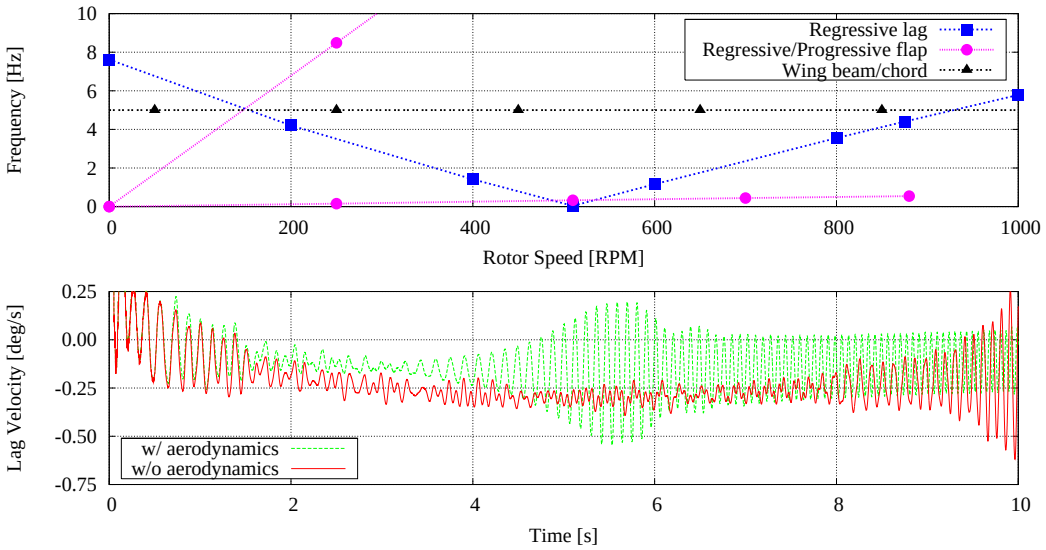

Figure 18: Lead-lag angular velocity during RPM sweep at 10 deg collective.

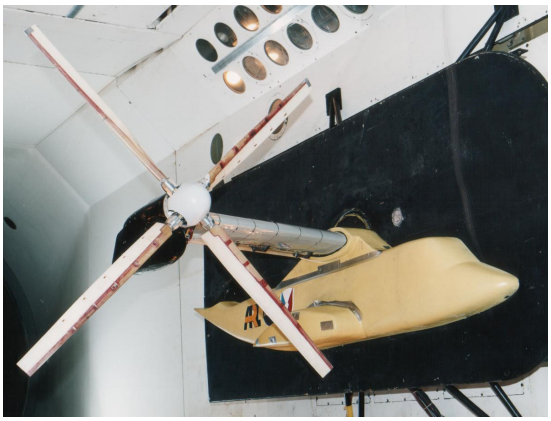

Figure 19: WRATS SASIP in forward flight configuration in the Transonic Dynamics Tunnel (TDT) at LaRC.

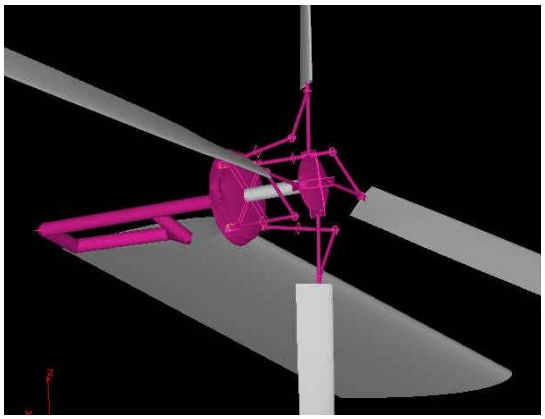

Figure 20: WRATS SASIP model in forward flight configuration.

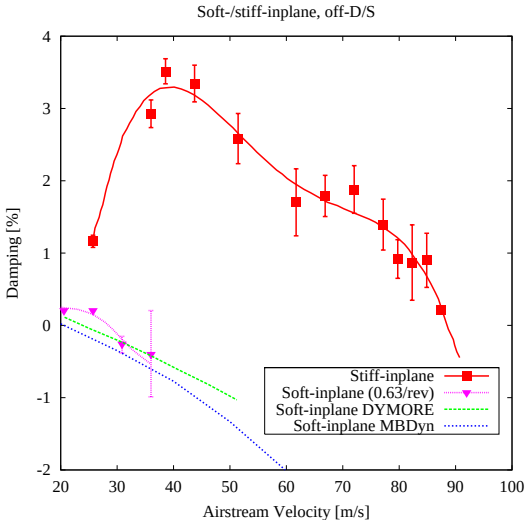

Figure 21: Wing beam bending mode damping comparison between original stiff-inplane WRATS model and SASIP soft-inplane model.

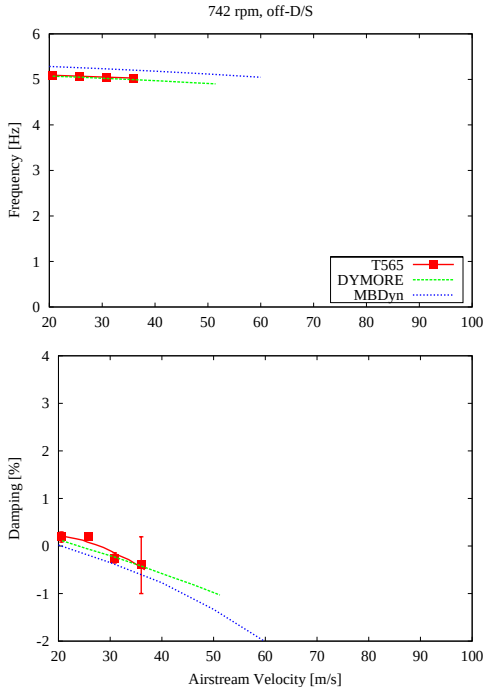

Figure 22: Wing beam bending mode frequency and damping comparison between experimental and numerical solutions at 742 RPM, off-D/S in windmill.

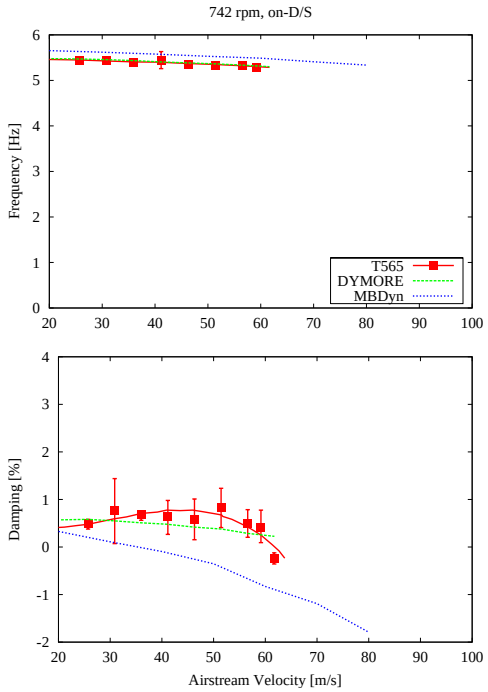

Figure 23: Wing beam bending mode frequency and damping comparison between experimental and numerical solutions at 742 RPM, on-D/S in windmill.

system and of its boundary conditions perfectly fit th assumptions. Briefly, the modal analysis of the wing and pylon subsystem has been performed including the hub and blade masses; then, the modal mass of the hub has been removed, resulting in modal shapes that account for the hub inertia, while the hub mass is modeled by the multibody portion of the analysis.

Figures 21–23 show MBDyn predictions with the same wing structural damping defined for the DYMORE model, i.e. 0.65%, on all modes. The unsteady aerodynamic loads on the wing are modeled by means of a Reduced Order Model (ROM), a state-space approximation of the generalized modal aerodynamic forces associated with the structural modes. The transfer function of the aerodynamic forces has been obtained using a linearized unsteady potential formulation based on the Morino method, a Boundary Element Method (BEM) that allows to keep into account the effect of the wing thickness; further details can be found in Ref. 9. Based on this data, a time domain realization is obtained using the best fit technique presented in Ref. 10. The wing beam bending mode resulting from this analysis is slightly less damped than in the experimental case, but the trends, with respect to airspeed, on/off-D/S and powered vs. windmill cases are confirmed.

Both analyses suffer from a lack of aerodynamic data, since the blade and wing airfoil characteristics are protected by confidentiality issues. However, it is believed that the use of generic aerodynamic properties does not significantly impact stability; only performances should be affected.

Airplane Mode Stability Issues

A first approximation of the drive train compliance entails the modeling of the shaft-hub interface by means of a spring and a damper, whose properties are to be determined empirically. The two limit cases of windmill and imposed RPM result by respectively assuming a null and an infinite stiffness. The former yields a lower damping of the wing beam bending mode, which, close to the stability boundary of the aeroelastic system, can be quantified in about 1% of the critical damping. This experimental result has been consistently obtained from both numerical analysis, with slight quantitative differences. Although no explanation of the mechanism that produces this effect has been inferred yet, the qualitative consistency between the analysis and the experiment suggests that the explanation is purely mechanical or aeroelastic, and is predictable by conventional analysis techniques. The analyses yield a difference between the powered and the windmill damping that is a bit less (between 0.2 and 0.4%) than what has been measured (above 1%). It was suggested that a possible expla-

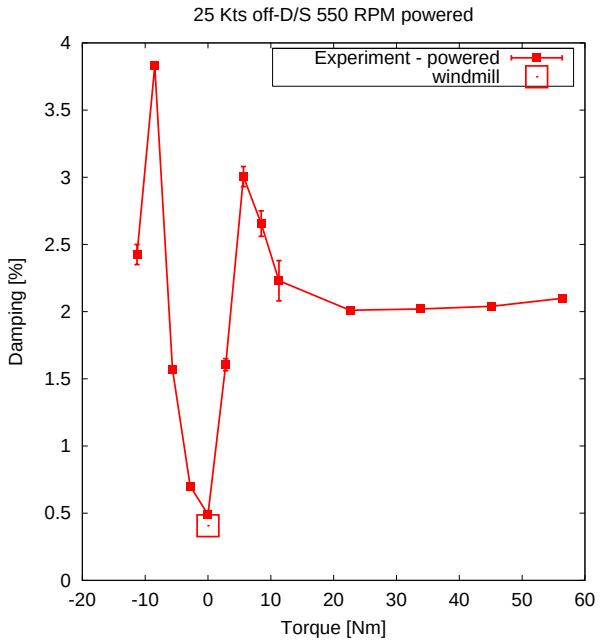

Figure 24: Wing beam bending mode damping in powered mode at 550 RPM, 25 Kts off-D/S; note the "bucket" close to zero torque.

nation could lie in the additional damping provided by the drive train, and the experimental evidence of higher damping of the imposed RPM case with respect to the numerical analysis, which is rather accurate in windmilling, seems to confirm it.

The experimental results also show the appearance of what has been termed a "damping bucket", i.e., at a given RPM and airstream speed, the damping of the wing beam bending mode shows a pronounced decrement at very low torque absolute values when running in powered mode, namely with the drive train connected to the hub. The minimum damping is obtained around zero net aerodynamic torque, and is comparable to that obtained in the windmilling case, as shown in Figure 24.

Since the phenomenon is completely ignored by the analyses presented in the previous paragraphs, a possible explanation has been sought in the nonlinear behavior of some components in the subsystem composed by the hub and the drive train.

When a high, yet finite shaft stiffness is used, the numerical analysis predicts stability margins comparable with those obtained at imposed hub RPM. If, on the contrary, a very low stiffness is used for the shaft, lower stability margins, comparable to those obtained in windmill conditions, have been computed. This suggested to explore the possibility of having a "deadband" in the shaft-hub connection, as illustrated in Figure 25, so that a very low equivalent stiffness results at low torque values, while a much higher stiffness results when

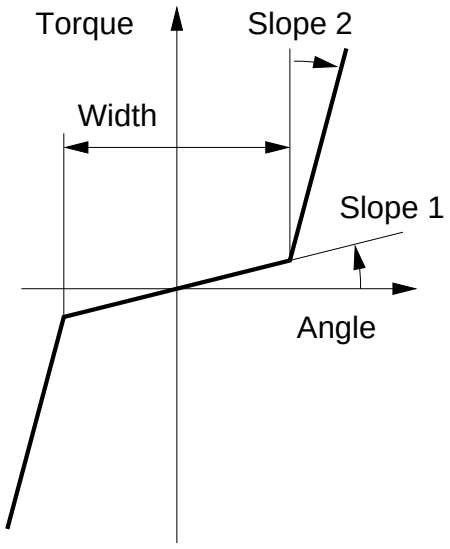

Figure 25: Sketch of the deadband in the drive train.

the deadband is not activated because of the bias torque that forces the system to work in the high stiffness region of the constitutive relation of the shaft.

An interesting result of the numerical analyses performed with the deadband effect on the shaft stiffness shows that when the drive train oscillation causes the system to "bump" against the deadband walls, the oscillations of the wing appear to be highly damped, as shown in Figure 26. After the amplitude of the oscillations is reduced, so that the drive train spring entirely works inside the low-stiffness region of the deadband curve, the damping of either the imposed RPM or of the windmill case is observed, and the damping bucket is predicted by the computation.

This suggests that the increased damping that appears at the ends of the bucket in the experimental measures might be the result of the "bumping" against the bucket walls, which would eventually disappear as the amplitude of the oscillations reduces below a threshold. This threshold can be used to determine the low stiffness inside the bucket. The identification of the parameters of the system may occur according to the following guidelines:

1. determine the stiffness of the drive train ("Slope 2" in Figure 25) far from the zero-torque condition by direct measurements and frequency calibration;

2. determine the width of the deadband ("Width" in Figure 25) by direct measurement of the freeplay;
3. measure the amplitude of the bucket (e.g. from Figure 24) in terms of torque, which is essentially proportional to the collective pitch angle. The stiffness inside the bucket is then obtained by dividing

the torque range inside the bucket by the oscillation amplitude that is just below the highly damped level.

The encouraging results obtained with this analysis are driving toward further investigation of the nonlinear dynamics of the drive system.

Computational Aspects

The two multibody analyses considered in this work present common aspects and some differences. The approach to the analysis of rotorcraft systems is basically analogous; it is partially different from usual comprehensive rotorcraft analysis, since it is essentially based on performing a *virtual experiment*: a detailed, nonlinear model of the rotorcraft system is analyzed by repeatedly performing time integration of Initial Value Problems (IVP), and synthetic information, like thrust or torque levels, blade angles at trim and so are obtained by averaging the results of the system response, or by letting it reach a steady solution, if any. Modal analysis follows different approaches.

DYMORE uses an *implicit matrix method* that exploits the properties of the Arnoldi's algorithm, a subspace method, which needs only a matrix-vector multiplication to extract the highest modulus eigenvalues of a discrete system, e.g. those that lie outside the unit circle in the complex plane (Ref. 11).

MBDyn, instead, uses the *Proper Orthogonal Decomposition* (POD) to extract a set of basis functions, called *Proper Orthogonal Modes* (POM), from the results of the numerical simulations. They are subsequently used in a Galerkin projection that yields low-dimensional dynamical models. The POMs are a minimal set of output signals that can be used to identify the dominant eigenvalues of the transition matrix (Refs. 12, 13). The numerical integration of the underlying IVP is performed by means of an original implicit multistep integration scheme, that guarantees second-order accuracy with tunable algorithmic dissipation.

Either of the two techniques is required because the detailed tiltrotor multibody model can be quite large; for instance, the complete MBDyn model entails about 800 unknowns, and models with as much as 2000 unknowns can be quite common. The virtual experiment approach requires the execution of long runs, so its feasibility heavily relies on the efficiency of the software. The codes used in this work proved to be able to perform the required computations, with rather realistic and detailed models, in reasonable times, as shown in Table III, along with other interesting figures.

Table III: Numerical Analysis Figures

Data	**DYMORE**	**MBDyn**
Model equations	∼1600	∼800
Beam el./blade	5	5
DoF/blade	48	132
Wing modes	—	5
Wing beam el.	4	—
Time step	0.001 s	0.001–0.0005 s
Time steps/rev	68–109	80–160
Real/sim. time	∼635:1	∼45:1
Computer	Xeon 1.7GHz	Athlon 2200+

The analysis of specific configurations and flight regimes may require the determination of non-trivial trim points. This work required the analysis of two significant cases: the windmill and the powered condition.

Windmill: this operational regime is defined by the collective setting that allows to maintain constant RPM with no power, which is unknown; so, to obtain the trim point, a low-gain controller that corrects the collective based on the integral of the RPM error has been implemented. A simplified form of the mast equilibrium equation is

$$J\dot{\Omega} = -C.$$

Its linearization yields

$$J\dot{\Omega} + \frac{\partial C}{\partial \Omega}(\Omega - \Omega_0) + \frac{\partial C}{\partial \theta}(\theta - \theta_0) = -C, \qquad (1)$$

where the sensitivities of the torque C to the angular velocity Ω and the collective θ are both positive. The controller equation is

$$\dot{\theta} = G(\Omega - \Omega_0),$$

which, combined with Eq. (1), normalized by the inertia J, yields

$$\begin{Bmatrix} \dot{\Omega} \\ \dot{\theta} \end{Bmatrix} = \begin{bmatrix} -\hat{C}_{/\Omega} & -\hat{C}_{/\theta} \\ G & 0 \end{bmatrix} \begin{Bmatrix} \Omega \\ \theta \end{Bmatrix} + \begin{Bmatrix} \hat{C}_{/\Omega}\Omega_0 + \hat{C}_{/\theta}\theta_0 \\ -G\Omega_0 \end{Bmatrix}.$$

It is stable provided positive gains G are considered, i.e. the collective increases when the rotating speed exceeds the nominal value and viceversa; the poles are

$$s = -\frac{\hat{C}_{/\Omega}}{2}\left(1 \pm \sqrt{1 - \frac{4\hat{C}_{/\theta}}{\hat{C}^2_{/\Omega}}G}\right).$$

The dominating one is that with the minus sign before the square root; for G small enough, it can be approximated by

$$s \cong -\frac{\hat{C}_{/\theta}}{\hat{C}_{/\Omega}}G;$$

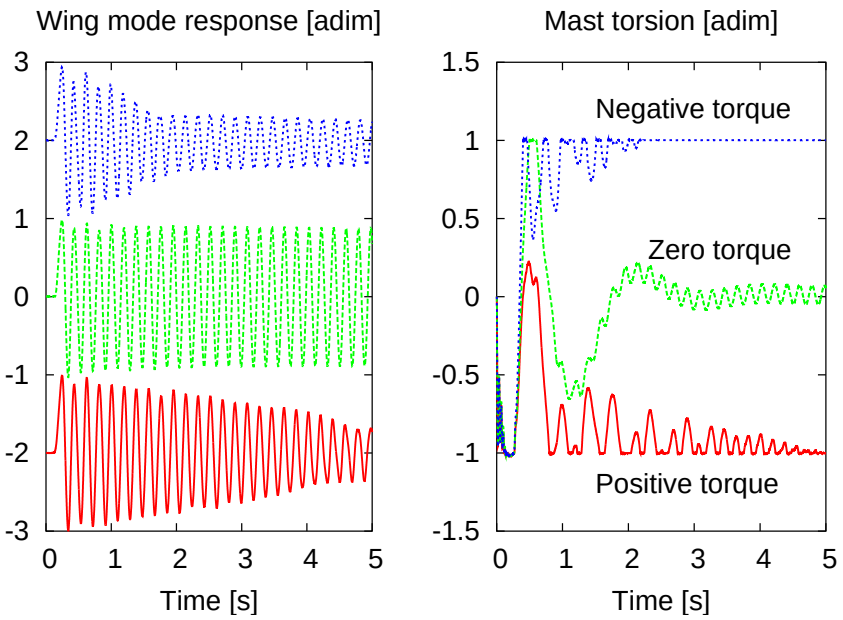

Figure 26: Wing beam bending mode when approaching zero-torque with a deadband on the drive train; note a higher apparent damping when the spring is working close to the region where the stiffness changes abruptly, possibly determining the peaks in the measured damping at the borders of the "bucket" in Figure 24

.

this eigenvalue dictates the time constant. Note that $C_{/\theta}$ depends on the square of the airstream speed, while $C_{/\Omega}$ is virtually independent from it; as a consequence, the time constant $\tau = -1/s$ for a given gain G decreases as the airstream increases. Time constants above 1 s have been used, to clearly separate the dynamics of the governor from the wing dynamics, in general above 5 Hz. The controller drives the collective to the value that corresponds to zero thrust in a relatively short time (10–30 revolutions, depending on the airstream speed through the sensitivity of the aerodynamic torque to collective changes), while preserving the windmill degree of freedom of the hub.

Powered: this operational regime has been simulated in two different manners. First, a setup analogous to that of the windmill regime has been used, with the desired torque applied between the shaft and the pylon. As a consequence, the controller drives the collective to a value that provides an aerodynamic torque equal to the applied one, while preserving the RPM. This case represents a powered trim point with the windmill degree of freedom still in place. Another case has been analyzed, consisting in imposing the RPM, thus eliminating the windmill degree of freedom, with the collective setting found above. This latter case corresponds to an infinite gain governor.

As a general trend, it is observed that the presence of some torque has a slightly stabilizing effect, which increases further by imposing the RPM. Apparently, of the two powered cases ranging from powered trim with windmill degree of freedom to infinite gain governor, the latter is more representative of the WRATS SASIP wind-tunnel model.

Concluding Remarks

This study shows that multibody codes can be successfully used to model complex mechanisms in rotorcraft analysis and that this capability can improve predictions of dynamic behavior. How this improved modeling capability can influence load and stability predictions is an anticipated conclusion which has not yet been resolved. Key points that highlight the importance of exploiting the capabilities of multibody analysis software are:

- hub and blade root kinematics and dynamics
- control system kinematics and structural dynamics
- finite element and composite-ready blade structural modeling
- versatility in structural modeling of unusual components
- essential rotor aerodynamics capabilities

The two multibody analysis software show analogous capabilities when applied to rotorcraft modeling. They are both able to capture the essential aspects of the whirl flutter stability of the WRATS SASIP wind-tunnel model, although the relatively inaccurate wing aerodynamic models available, and some uncertainty on the level of structural damping, did not allow, in some specific case, to obtain consistent quantitative whirl flutter predictions. The availability of two independently developed and validated multibody models of the WRATS SASIP represents an opportunity for future investigation of the aeromechanics of soft-inplane tiltrotor systems.

Acknowledges

The Authors wish to acknowledge Dr. Mark W. Nixon and Professors Giampiero Bindolino and Paolo Mantegazza for their contribution to the experimental investigations and the multibody formulation this work is based on.

References

[1] David J. Piatak, Raymond G. Kvaternik, Mark W. Nixon, Chester W. Langston, Jeffrey D. Singleton, Richard L. Bennett, and Ross K. Brown. A wind-tunnel parametric investigation of tiltrotor whirl-flutter stability boundaries. In *American Helicopter Society* 57^{th} *Annual Forum*, Washington, DC, May 9–11 2001.

[2] Mark W. Nixon, Chester W. Langston, Jeffrey D. Singleton, David J. Piatak, Raymond G. Kvaternik Lawrence M. Corso, and Ross Brown. Aeroelastic stability of a soft-inplane gimballed tiltrotor model in hover. In *AIAA/ASME/ASCE/AHS/ASC Structures, Structural Dynamics and Materials Conference*, Seattle, WA, April 16–19 2001.

[3] Gian Luca Ghiringhelli, Pierangelo Masarati, Paolo Mantegazza, and Mark W. Nixon. Multi-body analysis of a tiltrotor configuration. *Nonlinear Dynamics*, 19(4):333–357, August 1999.

[4] Olivier A. Bauchau. Computational schemes for flexible, non-linear multi-body systems. *Multibody Systems Dynamics*, 2(2):169–225, 1998.

[5] G. Bir and Indeerit Chopra. *University of Maryland Advanced Rotor Code (UMARC) Theory Manual*. University of Maryland Center for Rotorcraft Education and Research, College Park, MD, November 1991.

[6] Pierangelo Masarati, David J. Piatak, Jeffrey D. Singleton, and Paolo Mantegazza. An investigation of soft-inplane tiltrotor aeromechanics using two multibody analyses. In *American Helicopter Society* 4^{th} *Decennial Specialists' Conference on Aeromechanics*, Fisherman's Wharf, San Francisco, CA, January 21–23 2004.

[7] Mark W. Nixon, Chester W. Langston, Jeffrey D. Singleton, David J. Piatak, Raymond G. Kvaternik, Lawrence M. Corso, and R. K. Brown. Aeroelastic stability of a four-bladed semi-articulated soft-inplane tiltrotor model. In *American Helicopter Society* 59^{th} *Annual Forum*, Phoenix, AX, May 6–8 2003.

[8] Gian Luca Ghiringhelli, Pierangelo Masarati, and Paolo Mantegazza. A multi-body implementation of finite volume beams. *AIAA Journal*, 38(1):131–138, January 2000.

[9] Giampiero Bindolino and Paolo Mantegazza. Improvements on a Green's function method for the solution of linearized unsteady potential flows. *Journal of Aircraft*, 24(6):355–361, 1987.

[10] Giovanni Pasinetti and Paolo Mantegazza. Single finite states modeling of aerodynamic forces related to structural motions and gusts. *AIAA Journal*, 37(5):604–612, May 1999.

[11] Olivier A. Bauchau and Yuri G. Nikishkov. An implicit transition matrix approach to stability analysis of flexible multi-body systems. *Multibody Systems Dynamics*, 5(3):279–301, 2001.

[12] Giuseppe Quaranta, Pierangelo Masarati, and Paolo Mantegazza. Dynamic characterization and stability of a large size multibody tiltrotor model by pod analysis. In *ASME* 19^{th} *Biennial Conference on Mechanical Vibration and Noise (VIB)*, Chicago Il, September 2–6 2003.

[13] Giuseppe Quaranta, Pierangelo Masarati, and Paolo Mantegazza. Assessing the local stability of periodic motions for large multibody nonlinear systems using POD. *Journal of Sound and Vibration*, 271(3–5):1015–1038, 2004.